

Proceedings Article

Heat dissipation and safety considerations during Lissajous scanning magnetic particle imaging

J. Wells^{1,*}, H. Paysen¹, O. Kosch¹, F. Wiekhorst¹

¹Physikalisch-Technische Bundesanstalt, Abbestraße 2-12, 10587 Berlin

*Corresponding author, email: james.wells@ptb.de

© 2020 Wells *et al.*; licensee Infinite Science Publishing GmbH

This is an Open Access article distributed under the terms of the Creative Commons Attribution License (<http://creativecommons.org/licenses/by/4.0>), which permits unrestricted use, distribution, and reproduction in any medium, provided the original work is properly cited.

Abstract

Magnetic particle imaging has undergone rapid development, and its capabilities have been demonstrated in a wide variety of preclinical applications. Despite this growing body of in-vivo work, little attention has so far been paid to the impact of MPI imaging sequences on tissue, and the potential short- and long-term health implications. It is common within the MPI community to refer to the technique as being neither invasive, toxic, ionizing, nor damaging. However, little experimental work has been undertaken to verify these claims. Here, we present an experimental and theoretical study of the heat dissipation occurring during 3D imaging within a Lissajous scanning MPI device.

1 Introduction

Magnetic particle imaging (MPI) has undergone rapid development of technological capabilities and applications. The common mantra expounded within the MPI community is that the technique is non-invasive, non-toxic and non-damaging [1]. This is based upon MPI's lack of ionizing radiation, use of biocompatible iron-oxide nanoparticles, use of lower-frequency magnetic fields than magnetic hyperthermia therapy, and short single-frame image acquisition times. While these assumptions are well grounded, they do not provide a complete picture of all the necessary considerations for assessing MPI safety, and they fail to consider the full set of circumstances in which the technology is currently finding implementation. In particular, if MPI is to find market approval for use in humans (outside of terminal patients), then the potential for short- and long-term damage infliction must be properly assessed, and safe limits for its operation ascertained [2].

While different MPI scanner designs have been

demonstrated, all involve some form of spatially resolved dynamic magnetization measurement. These are normally achieved through the superposition of one or more AC excitations with a static gradient field. Despite the relatively low frequencies used in MPI, the imaging sequences in all scanners will induce accelerated levels of dissipative Néel and Brownian relaxation events, and some level of heat generation.

Temperature increases caused by magnetic field exposures result from the balance between MNP heating efficiency, type of magnetic field sequence used, length of field exposure, and rate of heat loss from the MNP impregnated region [3]. Furthermore, even in the absence of macroscopic heating effects, nanoscale effects in the vicinity of nanoparticles can generate sufficient disruption to harm cells [4].

It was previously highlighted that a correlation exists between the production of strong MPI imaging signals (MPS spectra), and strong magnetic hyperthermia heating effects (1D excitation) [5]. In this study, we focus on the heating which occurs during 3D imaging within a Lis-

sajous scanning field-free-point MPI scanner. Heating effects in a different type of scanner were briefly studied in [6].

II Material and methods

Details of the equipment and model used in the study follow.

II.I MPI scanner and calorimetry

All MPI measurements were conducted using the same preclinical MPI scanner (Bruker 25/20 FF). The device operates based on a Lissajous-scanning field-free-point approach. The scanner provides AC drive fields (0-12 mT) with fixed frequencies of 24510/26042/25253 Hz in the x- y- z- axes respectively. The AC components can be combined with a variable static gradient field with maximum possible values of 1.25/1.25/2.5 T/m in the x- y- and z- directions.

To determine the extent of heating generated within the scanner, a 50 μL sample of nanoparticles ($c(\text{Fe}) = 72 \text{ mg/ml}$) was placed at the centre of the scanner's field-of-view, with a fiber-optic probe inside. The temperature was recorded during exposure to extended MPI imaging sequences.

II.II Magnetic Nanoparticles

RCL-01 iron oxide nanoparticles (Resonant Circuits, London) were employed as the tracer/heating agent in all measurements. The particles have an average hydrodynamic diameter of 149 nm, and exhibit MPS spectra with an A5/A3 ratio of 31.3.

II.III Specific absorption rate calculations

The corrected slope technique was used to calculate the specific absorption rate (heating power per unit mass nanoparticles) from calorimetry measurements.

$$SAR_{CST} = \frac{(C \frac{dT}{dt} + L\Delta T)}{m_{MNP}}$$

C = heat capacity, T = temperature, t = time, L = linear heat loss parameter, m_{MNP} = mass of nanoparticles in sample.

III Results and discussion

Experimental and modelling results are presented in the following sections.

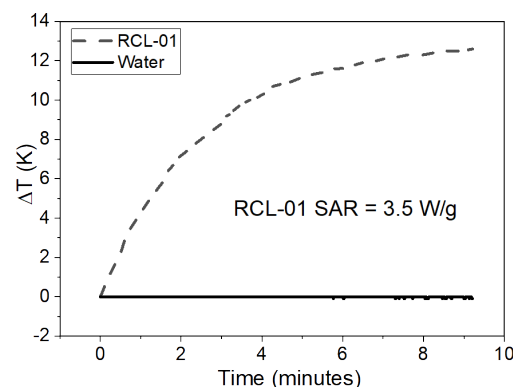


Figure 1: Calorimetry measurements of 50 μL RCL-01 and water samples when located at the centre of the scanner's field-of-view during exposure to 3D imaging field (3D 12 mT, 2.5 T/m).

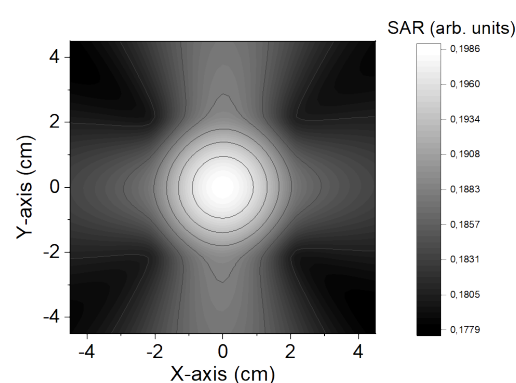


Figure 2: Simulation of the spatial dependence of the specific absorption rate with the Lissajous scanner under typical 3D imaging conditions (12 mT excitation fields, 2.5 T/m field gradient, timestep 0.1 μs). The map shows a single plane in the x- y- axis located at $z = 0$.

III.I Scanner calorimetry

Calorimetry heating curves obtained from both a 50 μL sample of RCL-01, and a second pure water sample (control), when situated at the center of the MPI scanner's field-of-view are shown in Fig 1. In both cases, the sample was exposed for 9 minutes to the magnetic field sequence typically employed for high-resolution 3D MPI imaging in the scanner. The RCL-01 particles display strong heating, despite the sample's large surface-to-volume ratio. The water sample shows no temperature change, emphasizing that the heating observed in the RCL sample is exclusively due to nanoparticle hyperthermia, with no heating due to heat leaking from the scanner's electronics.

III.II SAR modelling

A simple model was developed to describe the heating generated by nanoparticles within the scanner. Assuming sufficiently large nanoparticles whose relaxation is

Brownian dominated at 25 kHz, the technique models the average torques τ exerted on the nanoparticle moments m by the magnetic field B at different locations within the scanner during a single 22 ms image acquisition sequence.

$$\tau = m \times B$$

An example of the SAR distribution prediction produced by the Brownian torque model is shown in Figure 2. The map shows a large hot-spot located around the centre of the scanner's FOV, which decays further away from the centre of the FOV.

IV Conclusions

We have presented results demonstrating that heat dissipation within a Lissajous MPI scanner can be both non-negligible and non-trivial. Using calorimetry measurements, we have shown significant heating of MNP within the scanner during typical MPI imaging sequences. The lengths of the exposures are comparable with those reported in the literature for signal averaging during in-vivo studies. Using a simple model, we have predicted the likely shape of the SAR spatial dependence within the scanner for Brownian dominated nanoparticles. Our results show that significant care should be taken when designing MPI imaging protocols, and that the safe limits for MPI imaging deserve to be studied in detail. Our work is currently being extended to include in-vitro studies of the impact of MPI exposure on human cancer cell populations.

Author's Statement

This project was supported by the DFG research grants "quantMPI: Establishment of quantitative Magnetic Particle Imaging (MPI) application oriented phantoms for preclinical investigations" (grant TR 408/9-1) and "Matrix in Vision" (SFB 1340/1 2018, no 372486779, projects A02 and B02).

References

- [1] Zhou et al, "Magnetic Particle Imaging for Radiation-Free, Sensitive and High-Contrast Vascular Imaging and Cell Tracking". *Curr Opin Chem Biol.* 2018 Aug; 45: 131-138.
- [2] Wells et al. „Standardisation of magnetic nanoparticles in liquid suspension" *J. Phys D: 50, 38* (2017)
- [3] Andreu et al " Accuracy of available methods for quantifying the heat power generation of nanoparticles for magnetic hyperthermia" *Int. J. Hyper., 29, 8* (2013)
- [4] Wells et al. "Probing particle-matrix interactions during magnetic particle spectroscopy" *JMMM* 475, (2019)
- [5] Southern et al. "Observation of correlated magnetic particle imaging and magnetic hyperthermia metrics in iron oxide nanoparticles" *Proceedings of 9th IWMPi: 17-19 March 2019, New York* (2019)
- [6] Tay et al "Magnetic Particle Imaging-Guided Heating in Vivo Using Gradient Fields for Arbitrary Localization of Magnetic Hyperthermia Therapy" *ACS Nano* 2018, 12, 4, 3699-3713